Theoretical Survey of the Gas-Phase Reactions of Allylamine with Co^+

Yan Ma, Wenyue Guo,* Lianming Zhao, Songqing Hu, Jun Zhang, Qingtao Fu, and Xiangfeng Chen

College of Physics Science and Technology, China University of Petroleum, Dongying, Shandong 257061, People's Republic of China

Received: September 4, 2006; In Final Form: March 12, 2007

Density functional theory calculations have been carried out to survey the gas-phase reactions of allylamine with Co^+. The geometries and bonding characteristics of all the stationary points involved in the reactions have been investigated at the B3LYP/6-311++G(d,p) level. Final energies are obtained by means of the B3LYP/6-311+G(2df,2pd) single-point calculations. The performance of these theoretical methods is valuated with respect to the available thermochemical data. Co^+ strongly binds allylamine by forming a chelated structure in which the metal cation binds concomitantly to the two functional groups of the neutral molecule. Various mechanisms leading to the loss of NH_3, NH_2, C_2H_2, and H_2 are analyzed in terms of the topology of the potential energy surface. The most favorable mechanism corresponds to the loss of NH_3, through a process of C−N activation followed by a concerted β-H shift. The accompanying NH_2 elimination is also discussed. The loss of C_2H_2 is also favorable, through C−C activation and stepwise β-H shift, giving $Co^+(NH_2CH_3)$ and $Co^+H(NH_2CH_2)$ as the product ions. Various possible channels for the loss of H_2 are considered. The most favorable mechanism of the H_2 loss corresponds to a pathway through which the metal acts as a carrier, connecting a hydrogen atom from the methylidyne group of allylamine with a hydrogen atom of the terminal methylene group. The product ion of this pathway has a tricoordinated structure in which Co^+ binds to the terminal two Cs and N atoms of the NH_2CH_2CCH moiety.

1. Introduction

The gas-phase interaction of transition metal cations with organic and bioorganic compounds is one of the most important topics during the past years due to the importance of such systems in several fields.[1−6] Very often, metal cation association is accompanied by significant bond activation effects, which lead to specific fragmentations that are often of analytical utility.[7−11] Furthermore, these interactions are crucial in many biological processes, and as a consequence, many efforts have been devoted to the formation, intrinsic properties, and reactivity of organometallic complexes of biological relevance.[12−15] A promising approach to these problems can be done in the combined gas-phase theory−experiment studies, which have the advantage of providing information on the intrinsic reactivity of organometallic systems, without interference from medium.[4−6]

The allylamine functionality is found in a wide range of biologically active compounds,[16,17] and allylamines are also valuable synthetic intermediates for the preparation of α- and β-amino acids,[18a] alkaloids,[18b−e] and aza-carbohydrate derivatives.[18f,g] The formation and properties of poly(allylamine)−metal ion complexes in solution have been reported in the literature.[19,20] Surprisingly, similar studies considering the structure and energy of allylamine−metal complexes in the gas phase are scarce,[21] and the first experimental results of the gas-phase reactions between allylamine and ions derived from $Co(CO)_3NO$ have been published in the early 1980s.[21] The products associated with NH_3, NH_2, C_2H_2, and H_2 elimination in the chemistry of allylamine with Co^+ suggest the molecule actually reacts analogously to *n*-propylamine, i.e., via H_2 and alkene elimination.[21−24] However, the allyl group also has an interesting and important effect on the gas-phase reactions: Co^+ does not insert into the polar C−N bond of propylamine,[22−24] while evidence—elimination of NH_3 and NH_2—exists for the insertion of the metal ion into the C−N bond of allylamine.[21]

In this publication, we employ density functional theory (DFT) to investigate the reaction mechanisms of Co^+ with allylamine. This includes a complete illustration of all possible competing pathways for producing products via C−N, C−C, N−H, and C−H activations on the triplet potential energy surface (PES).

2. Computational Details

DFT in its three-parameter hybrid B3LYP functional[25,26] together with the 6-311++G(d,p) basis set was employed in the structural optimization for all the reactants, products, intermediates, and transition states involved in the reactions under consideration. This approach is known to yield reliable geometries for a wide variety of systems, including transition metal containing systems.[4−6,27−29] The harmonic vibrational frequencies of the optimized stationary points were calculated at the same level to estimate the zero-point energies (ZPE) that are included in all cited relative energies, to characterize the stationary points on the PES as local minima or transition states, and to generate the force constants needed for intrinsic reaction coordinate (IRC) calculations,[30] which were performed to identify pathways between the transition states and their connecting minima. For each structure obtained in this way, the single-point energy was computed using the B3LYP method with a larger basis set of 6-311+G(2df,2pd). Electron configurations as well as donor−acceptor stabilizations employed in the discussion were computed in the natural bond orbital analysis

* To whom correspondence should be addressed. E-mail: wyguo@hdpu.edu.cn.

10.1021/jp0657383 CCC: $37.00
Published on Web 06/22/2007

TABLE 1: Calculated and Experimental Binding Energies (in kcal/mol) at 0 K for Some Representative Species Involved in the Reactions of Co^+ with Allylamine

		calcd	
species	expt	method 1[a,b]	method 2[c,b]
Co^+-H	45.7 ± 1.4[d]	40.4 (-5.3 ± 1.4)	40.9 (-4.8 ± 1.4)
Co^+-CH_2	74.7 ± 1.4[e]	72.9 (-1.8 ± 1.4)	73.3 (-1.4 ± 1.4)
Co^+-CH_3	48.4 ± 0.9[d]	49.1 (0.7 ± 0.9)	49.5 (1.1 ± 0.9)
$Co^+-C_2H_2$	43 ± 2[f]	44.4 (1.4 ± 2)	45.1 (2.1 ± 2)
$Co^+-C_3H_4$	$>20.3 \pm 2.1$[e]	45.9	37.4
$^4[Co^+-C_3H_5]$	46.4 ± 4.2[e]	50.0 (3.6 ± 4.2)	49.7 (3.3 ± 4.2)
$^2[Co^+-C_3H_5]$		56.5 (10.1 ± 4.2)	49.5 (3.1 ± 4.2)
$^4[Co^+-NH_2]$	60.7 ± 2.1[g]	68.3 (7.6 ± 2.1)	67.8 (7.1 ± 2.1)
$^2[Co^+-NH_2]$		29.2	33.4
Co^+-NH_3	55.1 ± 3.8[h]	52.9 (-2.2 ± 3.8)	52.2 (-2.9 ± 3.8)
$C_3H_5-NH_2$		62.1	61.9
NH_2-H	107.3 ± 0.3[i]	103.7 (-3.6 ± 0.3)	104.0 (-3.3 ± 0.3)
CH_3NH-H	99.1 ± 2.5[i]	94.9 (-4.2 ± 2.5)	95.0 (-4.1 ± 2.5)
CH_3-NH_2	79.5[j]	77.6 (-1.9)	77.1 (-2.4)

[a] B3LYP/6-311++G(d,p). [b] Values in the parentheses are error bars of BDEs expected at the chosen levels of theory and were obtained by subtracting the experimental value from the calculated BDE. [c] B3LYP/6-311+G(2df,2pd)//6-311++G(d,p). [d] Reference 34. [e] Reference 35. [f] Reference 36. [g] Reference 37. [h] Reference 38. [i] Reference 39. [j] Reference 40.

(NBO) scheme.[31] We also detected the values of $\langle S^2 \rangle$ for all the calculated species to evaluate if spin contamination can influence the quality of the results. For species with large spin contamination, the internal and external stability of the DFT solution was calculated with the help of Hermitian stability maxtrices **A** and **B**.[32] All of the calculations were carried out using the GAUSSIAN 03 package.[33]

3. Results and Discussion

For transition metal containing systems, the possible crossing between surfaces corresponding to different spins should be taken into account. We have probed the first excited state—the quintet state—for several important reaction paths accompanying the Co^+ + allylamine reactions and found that this surface lies systematically higher than the triplet one (see Figure S1 in Supporting Information), suggesting that indeed no crossing takes place between the surfaces. Thus we only focus our study on the triplet surface (the ground surface).

In the following sections, we will first establish the accuracy that can be expected from the levels of theory chosen for the Co^+/allylamine system. Then, we will examine the title reactions in detail, including geometries of various stationary points and PES profiles for all possible product channels.

3.1. Calibration. In order to evaluate the general reliability of the levels of theory chosen, we carried out a study with a comparison of experimentally known binding energies (BDE)[34−40] with results from the B3LYP calculations for a set of representative species relevant to the title reactions. Table 1 collects the theoretically predicted BDEs and the most reliable experimental data for these species. Given in the parentheses are error bars for the calculated BDEs expected at the employed levels of theory, which are obtained from the subtraction of the calculated BDEs by the experimental values. As shown in Table 1, in most cases theoretical values are in good agreement with experimental findings. Although the errors of some parameters calculated at the B3LYP/6-311++G(d,p) level are as large as 5.3 ± 1.4 to 10.1 ± 4.2 kcal/mol, the B3LYP/6-311+G(2df,-2pd)//6-311++G(d,p) values agree well with the experimental findings in most cases except Co^+-NH_2 (7.1 ± 2.1 kcal/mol).

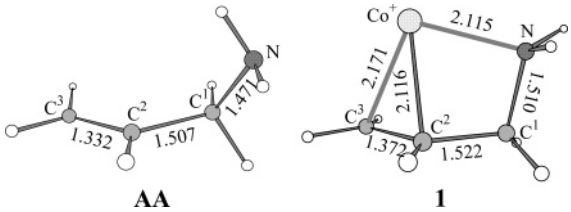

Figure 1. Optimized geometries and selected structural parameters for allylamine (**AA**) and the allylamine−Co^+ complex. Bond lengths are in angstroms and bond angles in degrees.

These facts validate the ability of the chosen level of theory to describe the features of the [Co, N, C_3, H_7]$^+$ PES.

Spin contamination was also checked for all the DFT solutions. Listed in Table S1 as Supporting Information are $\langle S^2 \rangle$ values before annihilation together with calculated total energies and ZPEs for all the species under study. It can be seen that in some cases the deviation of $\langle S^2 \rangle$ is larger than 10%. Taking into account that in DFT the value of $\langle S^2 \rangle$ is underestimated,[41] some instability in the wavefunction should be checked and corrected.[42] We made a stability test[32] for the geometries whose deviation of $\langle S^2 \rangle$ is larger than 5%, and we found that the wavefunction of most structures are stable, with the exception of the structure of *c*-$^2CoC_3H_5^+$, **5**, $^2CoC_3H_5^+$, and $Co^+(NCH_2CHCH_2)$, where an internal instability was detected for each of the DFT wavefunctions. For the former two, these unstable wavefunctions were then optimized, and on the basis of the optimized wavefunctions, the structures were reoptimized and the single-point energies were calculated in order to give more reliable results. However, for the later two, the optimization of wavefunction does not result in any remarkable changes in the results because the wavefunctions are nearly optimized.

3.2. Molecular Reactant and Encounter Complex. An exhaustive analysis of the allylamine conformations has identified five isomers with an almost identical energy for the molecule due to different orientations of the two functional groups.[43] In the present work, these conformers of allylamine are also located with the largest stabilization difference of 1.5 kcal/mol, suggesting the coexistence of the isomers in the gas phase. For convenience, the most stable structure of allylamine is selected in the discussion (**AA**; see Figure 1). Structures and relative energies (with respect to **AA**) for the other conformers (**AA1**−**AA4**) are given as Supporting Information (Figure S2).

In spite of these different conformations of the molecule, only one structure was found for the Co^+(allylamine) complex: **1**, as shown in Figure 1. This encounter complex is featured by a C_1 symmetry and a multicenter association of Co^+ with N, C^2, and C^3 of the molecule (R = 2.115, 2.116, and 2.171 Å, respectively), suggesting the comparable interactions of the metal with both the allylic-π and amido lone-pair orbitals. Correspondingly, the metal$^+$-allylamine BDE is calculated to be as large as 69.8 kcal/mol at the B3LYP/6-311+G(2df,2pd)//6-311++G(d,p) level. When attaching to Co^+, all the skeleton bonds of allylamine are stretched (by ~3% for C^2-C^3 and C^1-N, and ~1% for C^1-C^2; see Figure 1) and thus weakened. The strong multicenter association of the complex may provide an explanation for C−N and C−C activations, which give rise to the corresponding products, i.e., the NH_3, NH_2, and C_2H_2 loss as observed in the gas-phase experiments.[21]

To gain a deep insight into the above-mentioned structure, NBO analysis was carried out on **1**. The valence electrons of Co^+ are distributed as $(ad_{xy})^2(ad_{yz})^2(ad_{z^2})^2(ad_{xz})^1(ad_{x^2-y^2})^1$ to maintain the ^3F character, leading to a $^3A_1$ ground state of the

TABLE 2: Possible (1-1 through 4-8) and Unobserved (1-1′ through 3-1′) Products Together with the Calculated Reaction Energies (in kcal/mol) at 0 K Associated with the NH_3, NH_2, C_2H_2, and H_2 Loss in the Reactions of Co^+ with Allylamine

products	method 1[a]	method 2[b]
(**1-1**) $Co^+C_3H_4 + NH_3$	−31.1	−23.4
(**1-2**) *c*-$Co^+C_3H_4 + NH_3$	−4.8	−2.5
(**1-1′**) $Co^+NH_3 + C_3H_4$	−38.0	−38.2
(**1-2′**) $Co^+NH_3 + c$-C_3H_4	−11.8	−11.6
(**2-1**) $^2Co^+C_3H_5 + NH_2$	5.6	12.5
(**2-2**) *c*-$^2Co^+C_3H_5 + NH_2$	43.3	41.9
(**2-3**) $^4Co^+C_3H_5 + NH_2$	12.1	12.2
(**2-4**) *c*-$^4Co^+C_3H_5 + NH_2$	33.7	36.0
(**2-1′**) $^2Co^+NH_2 + C_3H_5$	32.8	28.6
(**2-2′**) $^2Co^+NH_2 + c$-C_3H_5	64.3	59.8
(**2-3′**) $^4Co^+NH_2 + C_3H_5$	−6.2	−5.9
(**2-4′**) $^4Co^+NH_2 + c$-C_3H_5	25.3	25.4
(**3-1**) $Co^+NH_2CH_3 + C_2H_2$	−23.7	−23.7
(**3-2**) $Co^+H(NH_2CH_2) + C_2H_2$	0.6	0.5
(**3-1′**) $Co^+C_2H_2 + CH_3NH_2$	−12.2	−12.8
(**4-1**) $Co^+(NHCHCHCH_2) + H_2$	−49.7	−47.5
(**4-2**) $Co^+(NH_2CH_2CCH) + H_2$	−32.0	−31.8
(**4-3**) $Co^+(NH_2CHCCH_2) + H_2$	−31.9	−30.3
(**4-4**) $Co^+(NCH_2CHCH_2) + H_2$	16.9	20.0
(**4-5**) $Co^+(NHCH_2CCH_2) + H_2$	4.9	6.8
(**4-6**) $Co^+(NHCH_2CHCH) + H_2$	−5.8	−4.4
(**4-7**) $Co^+(NH_2CH_2CHC) + H_2$	−5.8	−2.1
(**4-8**) $Co^+(NH_2CHCHCH) + H_2$	−23.0	−20.4

[a] B3LYP/6-311++G(d,p). [b] B3LYP/6-311+G(2df,2pd)//6-311++G(d,p).

complex. The multicenter structure of **1** favors not only the donation of the lone pair on N (n_N) into the metal 4s orbital (ΔE: 31.9 kcal/mol) but the well-known Dewar−Chatt model for the association of transition metal ions with alkenes also,[44] i.e., electron donation from the $\pi_{C^2C^3}$ orbital to the metal 4s orbital (ΔE: 41.9 kcal/mol) as well as that from the metal $d_{xy}d_{yz}$ mixture orbital to the $\pi^*_{C^2C^3}$ orbital (ΔE: 26 kcal/mol). It is these donor−acceptor interactions that result in the strong association of Co^+-allylamine and the weakening of the skeleton bonds of allylamine as well.

3.3. Gas-Phase Reaction Mechanisms. The ion cyclotron resonance (ICR) spectrum reported in ref 21 shows four neutral eliminations corresponding to NH_3, NH_2, C_2H_2, and H_2 in the gas-phase reactions of Co^+ with allylamine. Table 2 tabulates all possible products for these observed eliminations (products **1-1** through **4-8**) together with the unobserved products (products **1-1′** through **1-3′**) for comparison. Also given in the table are reaction energies (ΔE) calculated at both the B3LYP/6-311++G(d,p) and B3LYP/6-311+G(2df,2pd)//6-311++G(d,p) levels for these products. In the following we shall present a systematic survey of the [Co-**AA**]$^+$ PES to find the gas-phase reaction mechanisms associated with all these products.

3.3.1. Loss of NH_3 and NH_2. In the reactions of Co^+ with propylamine, prohibition of Co^+ insertion into the polar C−N bond is indicated by the absence of the corresponding products, which was supposed to be a result of a very weak Co^+−NH_2 bond (<18.7 kcal/mol).[22,23] However, Clemmer et al. found a value of 60.7 ± 2.1 kcal/mol for the Co^+−NH_2 BDE,[37] and we calculated it to be 67.8 kcal/mol using the B3LYP method (Table 1). Interestingly, evidence exists in the insertion of Co^+ into the C−N bond of allylamine: products of NH_2 and NH_3 were experimentally observed.[21,22] It was supposed that this may be because the Co^+−allyl bond alone is stronger than the C−N bond of allylamine, and insertion could occur even if the Co^+-NH_2 bond is very weak.[22] But according to our calculations, it is not the Co^+−allyl bond (BDE: 49.7 kcal/mol) but the Co^+−NH_2 bond (BDE: 67.8 kcal/mol) that is stronger than the C_3H_5−NH_2 bond (BDE: 61.9 kcal/mol).

Loss of NH_3 and NH_2 is found to follow the C−N activation of allylamine with Co^+ through two mechanisms, i.e., direct β-H migration and cyclization−hydrogen migration, whose PESs are shown in Figures 2 and 3, respectively, together with the schematic representations of the involved structures. For simplification, the information about these geometries is given as Supporting Information (see Figure S3). We can find that the reaction generally proceeds from the encounter complex **1** followed by the oxidative addition across the C−N bond by the metal ion to form the C−N insertion species **2** via saddle point $\mathbf{TS_{1-2}}$. This probability involves a low-energy pathway as reflected by the relative stabilities of the transition state and minimum involved (−41.4 and −58.5 kcal/mol for $\mathbf{TS_{1-2}}$ and **2**, respectively) due to the strong bonding of Co^+−allylamine as well as the strong Co^+−allyl and Co^+−NH_2 bonds as discussed above. On the other hand, such a process is also dynamically favored by two other factors: (1) the position of Co^+ in **1**, which is found to be located just above the C−N bond, and (2) the C−N stretching vibration, which is expected to be excited in the process of Co^+ binding to allylamine. In other words, in the Co^+ + allylamine reactions C−N activation is favorable both energetically and dynamically, which explains the experimental findings.[21] Once structure **2** is formed, two alternative mechanisms could lead to the elimination of NH_3, which will be discussed one by one in the following sections.

(a) Direct β-H Migration Mechanism. As shown in Figure 2, proceeding along this reaction coordinate, a one-step, concerted β-H migration can carry **2** to a dicoordinated ammonia−Co^+−propadiene complex (**3**) through a higher energy barrier ($\mathbf{TS_{2-3}}$) lying still ∼20 kcal/mol below the entrance channel. One feature of **3** is the overall C_s symmetry with the symmetry plane defined by N−Co^+−C^1−C^3. Owing to the strong interaction of Co^+ with both of the connected ligands, the new intermediate is quite stable, lying 71.2 kcal/mol below the entrance channel and constituting the global minimum of the [Co, N, C_3, H_7]$^+$ PES. Direct dissociation of **3** could give rise to $CoC_3H_4^+ + NH_3$ (product **1-1**), which is 23.4 kcal/mol lower in energy than the separated reactants.

(b) Cyclization−Hydrogen Migration Mechanism. From Figure 3, we can find that this mechanism implies a cyclization of the allyl group of **2** for forming the dicoordinated cyclopropyl−Co^+−amino complex **5** via $\mathbf{TS_{2-5}}$, in which the new C^1−C^3 bond is shortened to 2.036 Å. Complex **5** is 27.8 kcal/mol less stable than **2**, and the energy barrier of the **2** → **5** transfer is 36.5 kcal/mol. The subsequent reaction path from **5** is analogous to the direct β-H migration mechanism as discussed above, involving a concerted H migration transition state, $\mathbf{TS_{5-6}}$. The difference exists in that in this case the migrating hydrogen atom comes from the C^1H_2 group and, more importantly, $\mathbf{TS_{5-6}}$ lies 5.6 kcal/mol above the entrance channel and is 25.2 kcal/mol less stable than $\mathbf{TS_{2-3}}$, indicating this mechanism is less favorable than the direct β-H migration mechanism. The forward product from $\mathbf{TS_{5-6}}$ is intermediate **6**, a product-like complex between *c*-$CoC_3H_4^+$ and NH_3, which would eventually dissociate into *c*-$CoC_3H_4^+ + NH_3$ (**1-2**).

It is very clear that the more possible mechanism of the NH_3 loss occurs through an initial C−N activation followed by a concerted β-H shift and then a nonreactive dissociation (mechanism "a"), in accordance with the well-known β-H shift mechanism proposed by Allison et al.[21] Our calculations indicate

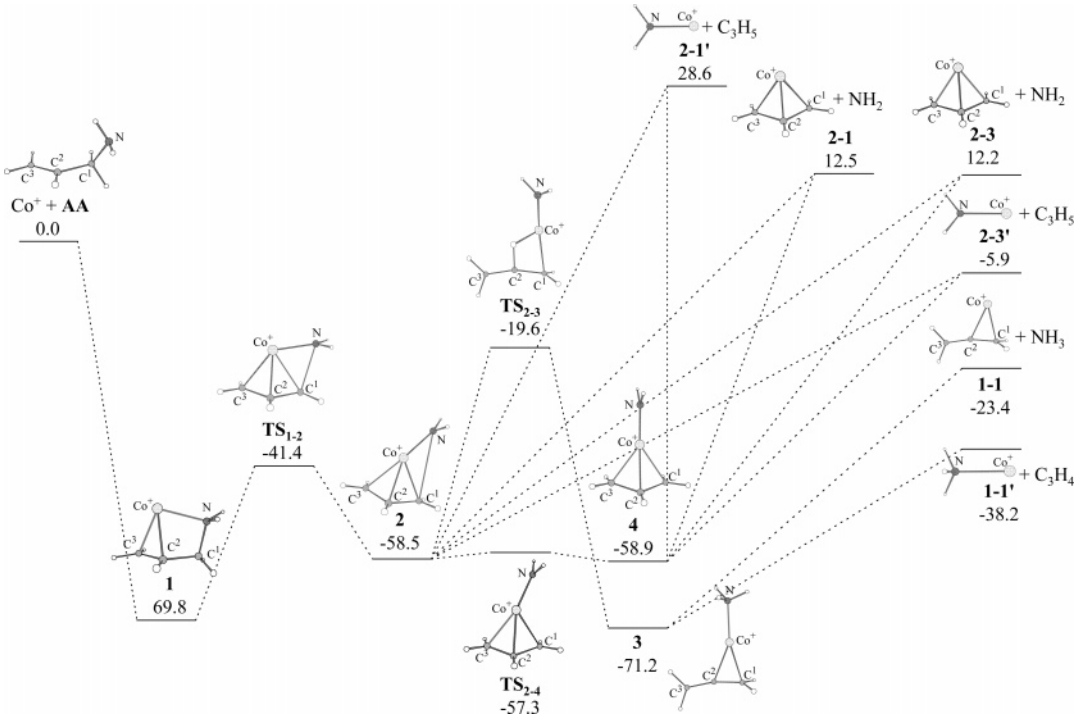

Figure 2. Energy profile for the direct β-H migration mechanism for the loss of NH_3 and NH_2. Numbers refer to the relative stability (in kcal/mol) with respect to the **AA** + Co^+ entrance channel evaluated at the B3LYP/6-311+G(2df,2pd)//6-311++G(d,p) level and includes ZPE corrections.

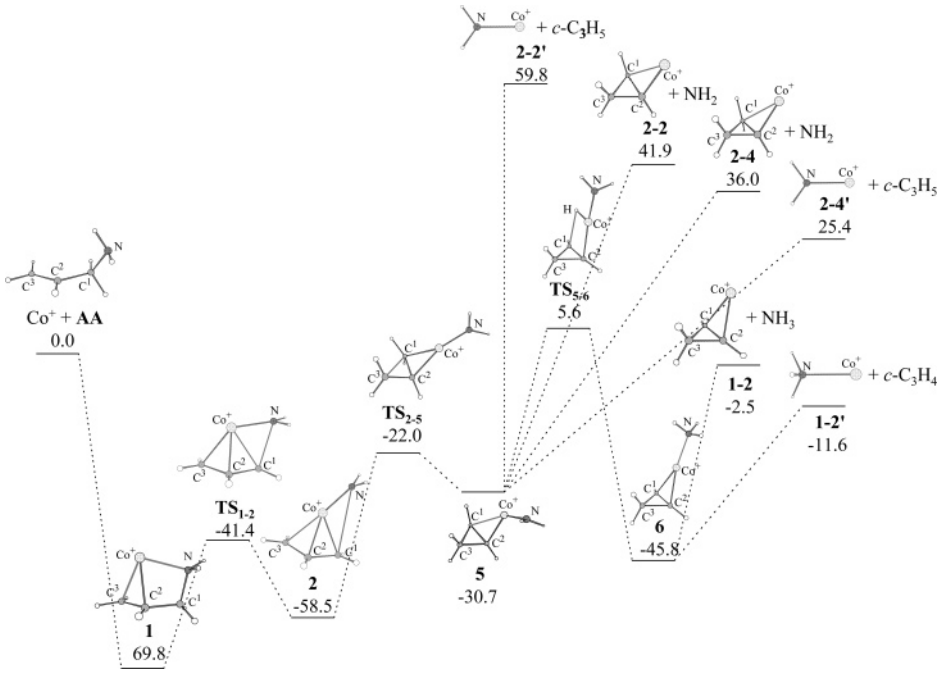

Figure 3. Energy profile for cyclization−hydrogen migration mechanism for the loss of NH_3 and NH_2. Energies follow the same notation as in Figure 2.

that the activation barrier of the β-H shift process is higher than that for the initial C−N activation. However, this mechanism is still the most favorable among all the Co^+ + **AA** reactions, since all the minima and transition states involved lie energetically far below the entrance channel.

It is important to note that although the alternative loss of C_3H_4 from **3** and **6** (leading to products **1-1′** and **1-2′**, respectively) is energetically preferable to these NH_3 losses, the products were not detected in the ICR experiment.[21] As a plausible explanation, the multicenter coordinate of Co^+ with C_3H_4 may hinder the excitation of the $Co^+-C_3H_4$ bond. On the other hand, the Co^+-NH_3 and Co^+-NH_2 bonds are expected to be excited readily in the above-mentioned conversion processes. Otherwise, a complete description of the experimental observation would require dynamical calculations that are out of the scope of this article.

NH_2 elimination must occur accompanying the loss of NH_3. For both the above-mentioned mechanisms, **2** and **5** could lead to the NH_2 elimination products directly. Also, the products could arise from species **4**, which is formed readily by a nearly barrier-free internal rotation of the NH_2 group of **2** that stabilizes the system by only 0.4 kcal/mol. Both **2** and **4** would decompose eventually into the NH_2 loss product $CoC_3H_5^+$ in its doublet and quartet states (i.e., **2-1** and **2-3**), which are endothermic by

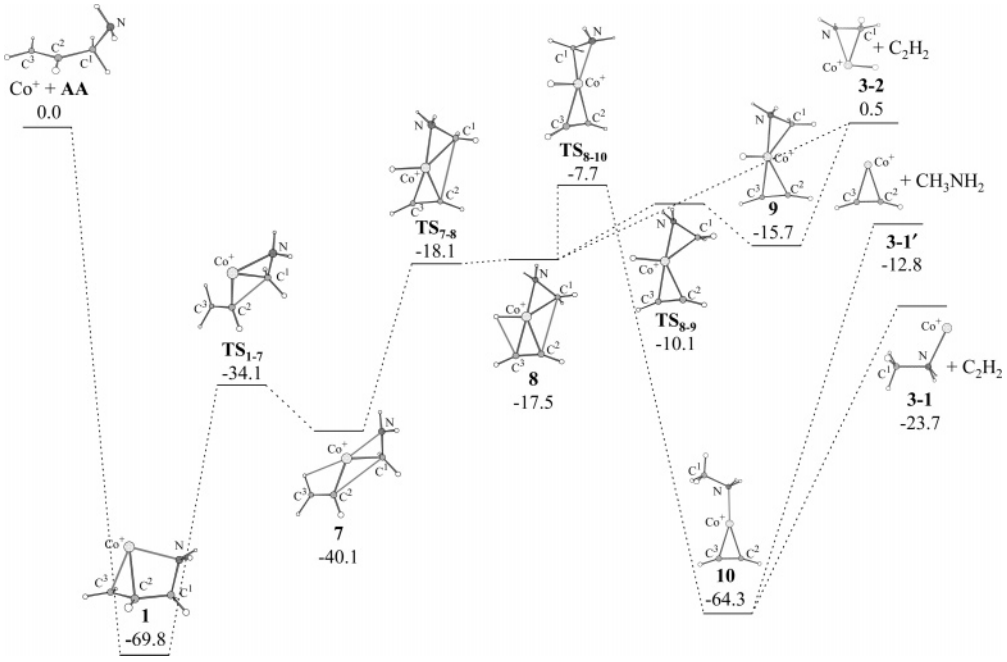

Figure 4. Energy profile for the loss of C_2H_2. Energies follow the same notation as in Figure 2.

12.5 and 12.2 kcal/mol, respectively, from the separated reactants. The alternative NH_2 loss products *c*-$CoC_3H_5^+ + NH_2$ could be produced from **5**, but they are strongly endothermic (by 41.9 and 36.0 kcal/mol for products **2-2** and **2-4**, respectively; see Table 2 or Figure 3).

3.3.2. Loss of C_2H_2. PES for this elimination is given in Figure 4 together with the schematic representations of the involved structures, and the information about these geometries is given as Supporting Information (see Figure S4). The C_2H_2 elimination channels follow initial C−C activation. Along this branch, encounter complex **1** is followed by intermediate **7**, in which Co^+ has inserted into the C^1-C^2 bond of allylamine. This possibility involves saddle point $\mathbf{TS_{1-7}}$ which is 7.3 kcal/mol higher in energy than the C−N insertion transition state ($\mathbf{TS_{1-2}}$) but still lies 34.1 kcal/mol below the entrance channel. Moreover, the new intermediate **7** is also rather stable (−40.1 kcal/mol). Thus, this C−C activation process is also possible. Subsequently, a β-H migration process that destabilizes the system by 22.6 kcal/mol would take place for **7**, converting into species **8**, which is featured by a tricoordination of Co^+ with the hydrogen, acetylene, and aminomethyl groups. It is worthy to note that such a tricoordinated structure is not found as a minimum in the above-mentioned NH_3 loss pathways as well as in the decarbonylation of acetaldehyde by Co^+.[4] The β-H migration process involves transition state $\mathbf{TS_{7-8}}$, which can be described as a late transition state, since its geometry is quite similar to that of **8**. Although $\mathbf{TS_{7-8}}$ has been confirmed to be the true first-order saddle point by IRC calculations, it is computed to lie 0.6 kcal/mol below **8** when ZPE corrections are included. This is due to the fact that the reported energies are obtained from single-point calculations with the larger 6-311+G(2df,2pd) basis set at the optimized B3LYP/6-311++G-(d,p) geometries.

Three possible exit channels could proceed from **8** by decompositions and rearrangements. The first one is that **8** directly decomposes into products $Co^+H(NH_2CH_2) + C_2H_2$ (**3-2**), which is almost thermoneutral from the separated reactants. The second one involves an intrarotation of the CH_2NH_2 group for **8** rearranging to a nearly isoenergetical species, **9**, via saddle point $\mathbf{TS_{8-9}}$ with an energy barrier of 7.4 kcal/mol. A direct dissociation of **9** could also give rise to product **3-2**. The third reaction channel involves a subsequent shift of the metal H of **8** that largely stabilizes the system (by 46.8 kcal/mol), leading to the very stable methylamine−Co^+−ethyne complex (**10**). This process implies an energy barrier of 9.8 kcal/mol ($\mathbf{TS_{8-10}}$), lying 7.7 kcal/mol below the entrance channel and constituting the highest energy barrier for all the C_2H_2 loss channels. Nonreactive dissociation of $(CH_3NH_2)Co^+-C_2H_2$ (**10**) would account for $Co^+(NH_2CH_3) + C_2H_2$ (**3-1**), which is exothermic by 23.7 kcal/mol with respect to the entrance channel. The alternative dissociation of **10** into $CoC_2H_2^+$ + methylamine (**3-1′**) is energetically 10.9 kcal/mol less favorable than the C_2H_2 elimination channel, in accordance with the fact that no methylamine loss products were observed in the ICR experiment.[21]

3.3.3. Loss of H_2. (a) "Direct" Mechanisms. The direct mechanisms for H_2 loss from two adjacent XH_2 groups through multicenter transition states have been established for alkane dehydrogenation reactions[45] and ethylenediamine + Cu^+ reactions.[6] For the allylamine + Co^+ reactions, in principle, three different mechanisms can be envisaged: the two eliminated hydrogen atoms come respectively from C^1N, C^1C^2, and C^2C^3. The schematic representations of the involved structures together with the PES for these product channels are given in Figure 5, and the information about these geometries is given as Supporting Information (see Figure S5). Even though the final products are quite stable, the energy barriers ($\mathbf{TS_{1-D1}}$, $\mathbf{TS_{1-D2}}$, and $\mathbf{TS_{1-D3}}$ for C^1N, C^1C^2, and C^2C^3 mechanisms) are too high, located above the entrance channel by 18.3, 34.2, and 40.4 kcal/mol, respectively.

(b) "Carrier" Mechanisms. Very often, transition metal cations act as "carriers" of hydrogen atoms in isomerization processes.[6] It can be envisaged that the reductive elimination of H_2 can proceed via insertion of the metal ion into the N−H and/or C−H bonds and isomerization of the insertion species by a subsequent hydrogen transfer.

Let us consider first the N−H activation channels. The schematic representations of the involved structures together with the PES involved in these product channels are given in Figure 6, and the information about these geometries is given

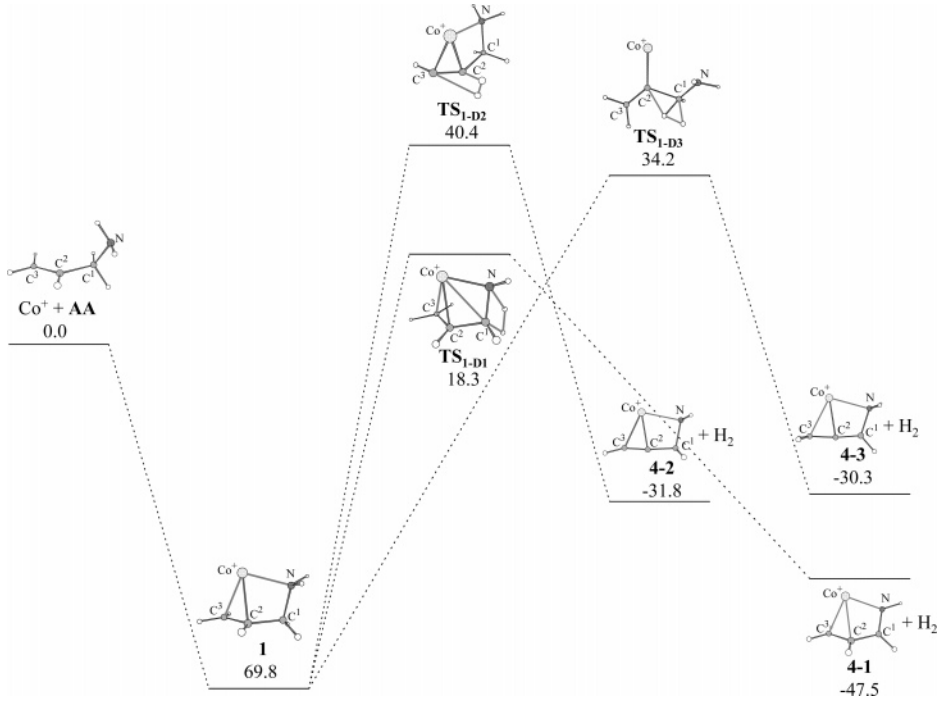

Figure 5. Energy profile for the reaction mechanisms corresponding to the direct loss of H_2 from adjacent XH_2 groups. Energies follow the same notation as in Figure 2.

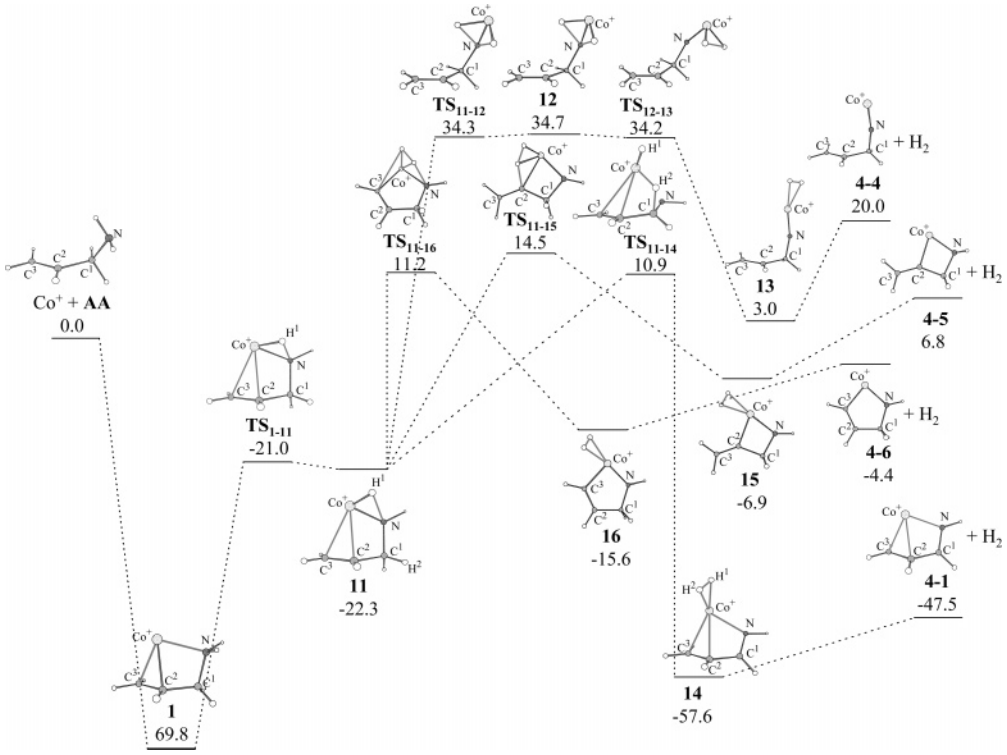

Figure 6. Energy profile for the "carrier" mechanism for the loss of H_2 in which initial N−H activation takes place. Energies follow the same notation as in Figure 2.

as Supporting Information (see Figure S6). The N−H insertion species (**11**) may be reached by the metal ion oxidative addition across one of the two N−H bonds of the encounter complex **1**. This process involves a "late" transition state (**TS$_{1-11}$**) that lies only 1.3 kcal/mol above **11** or 21.0 kcal/mol below the separated reactants. Once **11** is reached, four possible mechanisms can be envisaged depending on from where the second shifted H comes (i. e., C^1-C^3 or N). The first pathway involves a subsequent H shift from the N center, which includes a H abstraction process to form the $Co^+(H)_2(NCH_2CHCH_2)$ dihydro intermediate (**12**), a rearrangement process leading to $Co^+(H_2)(NCH_2CHCH_2)$ (**13**), and a nonreactive dissociation to give rise to $H_2 + Co^+(NCH_2CHCH_2)$ (**4-4**). This reaction pathway is identified as a high-energy channel because both the involved transition states (**TS$_{11-12}$** and **TS$_{12-13}$**) and the dihydro-complex **12** are located in a flat altiplano region (∼34 kcal/mol above the entrance channel) on the PES. The three other pathways are analogous to each other, i.e., involving a concerted H migration

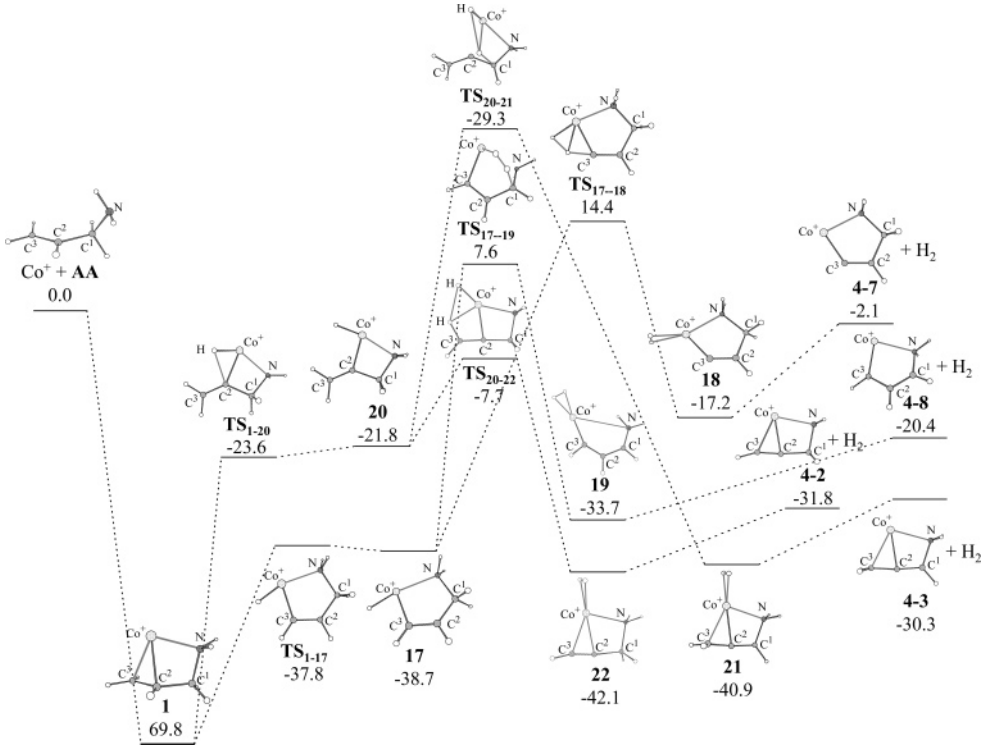

Figure 7. Energy profile for the "carrier" mechanism for the loss of H_2 in which initial C−H activation takes place. Energies follow the same notation as in Figure 2.

from the different C atom in **11** to form a molecular-hydrogen complex (**14**, **15**, or **16**) via a high-energy barrier (10.9, 11.2, and 14.5 kcal mol^{-1} above the entrance channel for $\mathbf{TS_{11-14}}$, $\mathbf{TS_{11-15}}$, and $\mathbf{TS_{11-16}}$, respectively). Nonreactive dissociation of these molecular-hydrogen complexes would give rise to dehydrogenation products (**4-1**, **4-5**, and **4-6**). Note that the **1** → **11** → **14** → **4-1** pathway is just the dehydrogenation mechanism proposed earlier for the reactions of Co^+ with allylamine,[22] which is not identified as a low-energy route in spite of the strong exthermicity of the resulting products (see Figure 6).

Now we turn to the other "carrier" mechanisms which involve initial C−H activations. The schematic representations of the involved structures for these product channels are given in Figure 7 together with the corresponding PES, and the information about these geometries is given as Supporting Information (see Figure S7). Two alternative mechanisms corresponding to initial 3- and 2-C−H activations were identified.

For the initial 3-C−H activation mechanisms, also starting from adduct **1**, one can reach a five-membered hydride complex, intermediate **17**, formed by Co^+ insertion into one C−H bond of the terminal CH_2 group. The probability involves transition state $\mathbf{TS_{1-17}}$, which is 16.8 kcal/mol lower in energy than the corresponding transition state for initial N−H insertion ($\mathbf{TS_{1-11}}$). Similar to the later one, this saddle point occurs very late on the reaction coordinate and bears already great structural similarity to the new structure **17**. After **17** is formed, two different channels noticed as 3,3- and 3,1-H_2 eliminations could be proceeded. The 3,3-H_2 elimination pathway from **17** involves a four-centered transition state, $\mathbf{TS_{17-18}}$, in which the second 3-H migration is taking place as reflected by the bond lengthening of the breaking C^3−H bond (1.376 Å) as well as that of the forming H−H bond (1.132 Å). The energy barrier of this process lies 14.4 kcal/mol above the entrance channel, much higher than the initial 3-C−H activation (by 53.1 kcal/mol). The forward product of $\mathbf{TS_{17-18}}$ is the molecular-hydrogen complex **18**, which dissociates directly into $Co^+(CCHCH_2NH_2) + H_2$ (**4-7**) without an activation barrier. The 3,1-H_2 elimination channel from **17** involves a subsequent 1-H migration to form intermediate **19** via a six-membered-ring transition state, $\mathbf{TS_{17-19}}$, which lies 6.8 kcal/mol below $\mathbf{TS_{17-18}}$ or 7.6 kcal/mol above the entrance channel. Similar to **18**, species **19** is also a direct precursor of the dehydrogenation products: $Co^+(CHCHCHNH_2) + H_2$ (**4-8**), which is calculated to be 20.4 kcal/mol exothermic from the separated reactants.

Now we consider the initial 2-C−H migration mechanisms. The 2-C−H insertion species (**20**) featured by an overall C_s symmetry can be formed through transition state $\mathbf{TS_{1-20}}$, which is 1.8 kcal/mol lower than the connecting minimum (**20**) due to the ZPE effects. Once **20** is formed, two different channels noted as 2,1- and 2,3-H_2 eliminations could also proceed. The 2,1-H_2 elimination involves a subsequent 1-H migration (from C^1) via transition state $\mathbf{TS_{20-21}}$, which assumes a much higher energy barrier (29.3 kcal/mol above the separated reactants). Therefore, this channel is energetically unfavorable. The exit channel of **21** is a simple dissociation into $Co^+(CH_2CCHNH_2) + H_2$ (**4-3**). The last and most important channel is 2,3-H_2 elimination, which is feasible to take place as the hydrogen attached to Co^+ is close enough to the H atom of the terminal CH_2 group. This possibility involves a low-energy barrier ($\mathbf{TS_{20-22}}$), lying 7.7 kcal/mol below the separated reactants. The forward product from $\mathbf{TS_{20-22}}$ is intermediate **22**, a product-like complex whose exit channel is $Co^+(CHCCH_2NH_2) + H_2$ (**4-2**). The exothermicity of this dehydrogenation product is computed to be 31.8 kcal/mol.

In summary, 11 different pathways falling into the two catagories of "direct" and "carrier" mechanisms could lead to the loss of H_2 from allylamine. Most of these mechanisms involve at least one high-energy barrier located above the $Co^+ + \mathbf{AA}$ entrance channel. From Figure 7, it is clear that the 2,3-H_2 elimination mechanism is the most favorable because it is the only pathway in which all the involved minima and transition

states are located below the entrance channel. It should be pointed out that this mechanism contrasts with the earlier proposed mechanism[22] as mentioned above, but it is analogous to the experimental findings of the reactions of Co^+ with a large set of labeled isotopomers of *n*-propylamine[24] in which the eliminated H_2 originates from the β and γ positions (corresponding to C^2 and C^3 in allylamine) of the propyl chain, respectively.

4. Conclusions

In this paper we have presented several mechanisms for the allylamine + Co^+ reactions, whose energy profiles are compatible with the observed loss of NH_3, NH_2, C_2H_2, and H_2.[21]

The approach of Co^+ toward different conformational isomers of allylamine only leads to one structure of the encounter complex in which the metal cation strongly binds to both functional groups of allylamine to form a chelated structure.

The most favorable mechanism corresponds to the direct β-H migration mechanism for the loss of NH_3, which occurs through Co^+ insertion into the C−N bond followed by a β-H shift and then a nonreactive dissociation process. This reaction path is favorable, because the energies of all the involved minima and transition states are located far below the entrance channel. The more complex and energetically less-favorable NH_3 elimination channel involves also C−N activation, H shift, and nonreactive dissociation, but in this case the system experiences a high-energy cyclization process immediately following the C−N activation. NH_2 elimination also comes from the C−N activation, but all the channels are endothermic.

The C_2H_2 elimination proceeds according to C−C insertion followed also by a β-H migration mechanism. However, in this case the H shift is a (two-step) stepwise process, resulting in the ionic products of $Co^+NH_2CH_3$ and $HCo^+(NH_2CH_2)$ as the C_2H_2 partners.

All possible H_2 loss mechanisms have been surveyed. Most of them experience at least one high-energy barrier located above the Co^+ + **AA** entrance channel. The most favorable dehydrogenation mechanism corresponds to 2,3-H_2 elimination. In the first step of this mechanism a migration of the methylidyne hydrogen of allylamine toward the metal takes place. In the subsequent steps the CoH group interacts with one of the terminal methylene hydrogens, leading to the loss of H_2 finally. The product ion has a tricoordinated structure in which Co^+ binds to the terminal two Cs and N atoms of the NH_2-CH_2-C-CH moiety.

Acknowledgment. This work was supported by SRF for ROCS, NCET-05-0608, Excellent Young Teachers Program, and Key Project (No. 104119) of MOE, P.R.C., National Natural Science Foundation of China (No. 20476061), and Natural Science Foundation of Shandong Province (No. Y2006B35).

Supporting Information Available: Quintet potential energy surfaces for the most important reaction mechanisms associated with the loss of NH_3, NH_2, C_2H_2, and H_2, optimized structures and relative energies for the conformational isomers of allylamine, optimized geometries and selected structural parameters for all the intermediates, saddle points and products for the loss of NH_3, NH_2, C_2H_2, and H_2, and total energies, zero-point energies, and values of $\langle S^2 \rangle$ for all the relevant species. This material is available free of charge via the Internet at http://pubs.acs.org.

References and Notes

(1) Haynes, C. L.; Fisher, E. R.; Armentrout, P. B. *J. Am. Chem. Soc.* **1996**, *118*, 3269.
(2) Burnier, R. C.; Byrd, G. D.; Freiser, B. S. *J. Am. Chem. Soc.* **1981**, *103*, 4360.
(3) Georgiadis, R.; Fisher, E. R.; Armentrout, P. B. *J. Am. Chem. Soc.* **1989**, *111*, 4251.
(4) Zhao, L. M.; Zhang, R. R.; Guo, W. Y.; Wu, S. J.; Lu, X. Q. *Chem. Phys. Lett.* **2005**, *414*, 28.
(5) Zhao, L. M.; Guo, W. Y.; Zhang, R. R.; Wu, S. J.; Lu, X. Q. *ChemPhysChem* **2006**, *7*, 1345.
(6) Alcamí, M.; Luna, A.; Mó, O.; Yáñez, M. *J. Phys. Chem. A* **2004**, *108*, 8367.
(7) Morizur, J.-P.; Desmazieres, B.; Chamot-Rooke, J.; Haldys, V.; Fordham, P.; Tortajada, J. *J. Am. Soc. Mass Spectrom.* **1998**, *9*, 731.
(8) Fordham, P.; Deschasse, M.; Haldys, V.; Tortajada, J.; Morizur, J.-P. *Eur. J. Mass Spectrom.* **2001**, *7*, 213.
(9) Gaucher, S. P.; Leary, J. A. *Anal. Chem.* **1998**, *70*, 3009.
(10) Dongré, A. R.; Wysocki, V. H. *Org. Mass Spectrom.* **1994**, 700.
(11) Sible, E. M.; Brimmer, S. P.; Leary, J. A. *J. Am. Soc. Mass Spectrom.* **1997**, *32*.
(12) Eichhorn, G. L. *Adv. Inorg. Biochem.* **1981**, 1.
(13) Sigel, A., Sigel, H., Eds. *Metal ions in biological systems*; Marcel Dekker: New York, 1996; Vols. 32 and 33.
(14) Karlin, D. K., Zubieta, J., Eds. *Biological and Inorganic Copper Chemistry*; Adenine Guiderland: New York, 1986; Vols. I and II.
(15) Whitfield, D. M.; Stojkovski, S.; Sarkar, B. *Coord. Chem. Rev.* **1993**, *122*, 171.
(16) Trost, B. M.; Crawley, M. L. *Chem. Rev.* **2003**, *103*, 2921.
(17) Trost, B. M. *Chem. Pharm. Bull.* **2002**, *50*, 1.
(18) Burgess, K.; Liu, L. T.; Pal, B. *J. Org. Chem.* **1993**, *58*, 4758. Ichikawa, Y.; Ito, T.; Nishiyama, T.; Isobe, M. *Synlett* **2003**, 1034. Ito, K.; Akashi, S.; Saito, B.; Katsuki, T. *Synlett* **2003**, 1809. Paquette, L. A.; Leit, S. M. *J. Am. Chem. Soc.* **1999**, *121*, 8126. Magnus, P.; Lacour, J.; Coldham, I.; Mugrage, B.; Bauta, W. B. *Tetrahedron* **1995**, *51*, 11087. Liu, H.; Liang, X.; Sohoel, H.; Buelow, A.; Bols, M. *J. Am. Chem. Soc.* **2001**, *123*, 5116. Trost, B. M.; Van Vranken, D. L. *J. Am. Chem. Soc.* **1993**, *115*, 444.
(19) Rivas, B. L.; Seguel, G. V. *Polym. Bull.* **1996**, *37*, 463.
(20) Rivas, B. L.; Perira, E. D. *Polym. Bull.* **2000**, *45*, 69.
(21) Lombarski, M.; Allison, J. *Int. J. Mass. Spectrom. Ion Phys.* **1983**, *49*, 281.
(22) Radecki, B. D.; Allison. J. *J. Am. Chem. Soc.* **1984**, *106*, 946.
(23) Babinec, S. J.; Allison, J. *J. Am. Chem. Soc.* **1984**, *106*, 7718.
(24) Karrass, S.; Prüesse, T.; Eller, K.; Schwarz, H. *J. Am. Chem. Soc.* **1989**, *111*, 9018.
(25) Becke, A. D. *J. Chem. Phys.* **1993**, *98*, 5648.
(26) Stephens, P. J.; Devlin, F. J.; Chabalowski, C. F.; Frisch. M. J. *J. Phys. Chem.* **1994**, *98*, 11623.
(27) Zhang, D. J.; Liu, C. P.; Bi, S.; Yuan, S. *Chem. Eur. J.* **2003**, *9*, 484.
(28) Jiang, N.; Zhang, D. J. *Chem. Phys. Lett.* **2002**, *366*, 253.
(29) Zhang, D. J.; Liu, C. P.; Bian, W. S. *J. Phys. Chem. A* **2003**, *107*, 8955.
(30) Gonzalez, C.; Schlegel, H. B. *J. Phys. Chem.* **1990**, *94*, 5523.
(31) Glendening, E. D.; Reed, A. E.; Carpenter, J. E.; Weinhold, F. NBO Version 3.1. Reed, A. E.; Curtiss, L. A.; Weinhold, F. *Chem. Rev.* **1988**, *88*, 899. Foster, J. P.; Weinhold, F. *J. Am. Chem. Soc.* **1980**, *102*, 7211.
(32) Bauernschmitt, R.; Ahlrichs, R. *J. Chem. Phys.* **1996**, *106*, 9047. Seeger, R.; Pope, J. A. *J. Chem. Phys.* **1977**, *66*, 3045.
(33) Frisch, M. J.; Trucks, G. W.; Schlegel, H. B.; Scuseria, G. E.; Robb, M. A.; Cheeseman, J. R.; Montgomery, J. A., Jr.; Vreven, T.; Kudin, K. N.; Burant, J. C.; Millam, J. M.; Iyengar, S. S.; Tomasi, J.; Barone, V.; Mennucci, B.; Cossi, M.; Scalmani, G.; Rega, N.; Petersson, G. A.; Nakatsuji, H.; Hada, M.; Ehara, M.; Toyota, K.; Fukuda, R.; Hasegawa, J.; Ishida, M.; Nakajima, T.; Honda, Y.; Kitao, O.; Nakai, H.; Klene, M.; Li, X.; Knox, J. E.; Hratchian, H. P.; Cross, J. B.; Adamo, C.; Jaramillo, J.; Gomperts, R.; Stratmann, R. E.; Yazyev, O.; Austin, A. J.; Cammi, R.; Pomelli, C.; Ochterski, J. W.; Ayala, P. Y.; Morokuma, K.; Voth, G. A.; Salvador, P.; Dannenberg, J. J.; Zakrzewski, V. G.; Dapprich, S.; Daniels, A. D.; Strain, M. C.; Farkas, O.; Malick, D. K.; Rabuck, A. D.; Raghavachari, K.; Foresman, J. B.; Ortiz, J. V.; Cui, Q.; Baboul, A. G.; Clifford, S.; Cioslowski, J.; Stefanov, B. B.; Liu, G.; Liashenko, A.; Piskorz, P.; Komaromi, I.; Martin, R. L.; Fox, D. J.; Keith, T.; Al-Laham, M. A.; Peng, C. Y.; Nanayakkara, A.; Challacombe, M.; Gill, P. M. W.; Johnson, B.; Chen, W.; Wong, M. W.; Gonzalez, C.; Pople, J. A. *Gaussian 03*, revision B.05; Gaussian, Inc.: Pittsburgh, PA, 2003.
(34) Haynes, C. L.; Armentrout, P. B. *Organometallics*. **1994**, *13*, 3480.
(35) Armentrout, P. B.; Kickel, B. L. In *Organometallic Ion Chemistry*; Freiser, B. S., Ed. Kluwer: Dordrecht, 1995; pp 1−45.
(36) Surya, P. I.; Ranatunga, D. R. A.; Freiser, B. S. *J. Am. Chem. Soc.* **1997**, *119*, 3351.
(37) Clemmer, D. E.; Armentrout, P. B. *J. Phys. Chem.* **1991**, *95*, 3084.

(38) Walter, D.; Armentrout, P. B. *J. Am. Chem. Soc.* **1998**, *120*, 3176.
(39) Lide, D. R. *CRC Handbook of Chemistry and Physics*; CRC Press: Boca Raton, FL, 2001. The experimental data were converted to the corresponding BDE in the gas phase at 0 K.
(40) Waschewsky, G. C. G.; Kitchen, D. C.; Browning, P. W.; Butler, L. J. *J. Phys. Chem.* **1995**, *99*, 2635.
(41) Gräfenstein, J.; Hjerpe, A. M.; Kraka, E.; Cremer, D. *J. Phys. Chem. A* **2000**, *104*, 1748. Gräfenstein, J.; Cremer, D. *J. Mol. Phys.* **2001**, *99*, 981.
(42) Alcamí, M.; Mó, O.; Yáñez, M.; Cooper, I. L. *J. Chem. Phys.* **2000**, *112*, 6131. Luna, A.; Alcamí, M.; Mó, O.; Yá˜nez, M. *Chem. Phys. Lett.* **2000**, *320*, 129.
(43) Herrebout, W. A.; Zheng, C.; Van der Veken, B. J.; Durig, J. R. *J. Mol. Struct.* **2003**, *645*, 109.
(44) Dewar, M. J. S**.** *Bull. Soc. Chim. Fr.* **1951**, *18*, C71. Chatt, J.; Duncanson, L. A. *J. Chem. Soc.* **1953**, 2939.
(45) Yi, S. S.; Blomberg, M. R. A.; Siegbahn, P. E. M.; Weisshaar, J. C. *J. Phys. Chem. A* **1998**, *102*, 395.